ASSESSMENT OF ATMOSPHERIC WATER VAPOR REMOTE SENSING USING GPS SIGNALS BY RADIOSONDE AND MODIS SATELLITE IMAGES

Bilal BELDJILALI[1], Salem KAHLOUCHE[1]

[1]Department of Space Geodesy, Center of Space Techniques, Algerian Space Agency, Arzew, Algeria
Corresponding author: bbeldjilali@cts.asal.dz

DOI: 10.5281/zenodo.4692723

Abstract. This paper is an evaluation of the atmospheric water vapor remote sensing by GPS signals. The integrated water vapor (*IWV*) is calculated based on the measurement of the tropospheric zenith total delay (*ZTD*) effects on the microwave signals emitted by GPS satellites. The methodology proposed in this work is based on the combination of the global navigation satellite system (GNSS) observations and navigation data from the international GNSS service (IGS) products with meteorological data, measured at the stations level, to calculate the *ZTD* delay and estimate the integrated water vapor value. This work was carried out using data records from12 IGS stations distributed in seven countries in the four seasons of the year. The obtained results are compared with the values generated by Radiosonde measurement and MODIS satellite images level 2 (Water Vapor data product). In more than 90% of cases, the difference between the GPS and Radiosonde solutions is less than 3 mm with a monthly RMS less than 1.6 and a correlation of about 95%. The comparison between the GPS and MODIS shows that in more than 65 % of the time, the difference between the two solutions is less than 4 mm with a monthly RMS less than 2.3, and the correlation is about 73%.

Key words: atmosphere remote sensing, troposphere, GNSS, zenith total delay, integrated water vapor, radiosonde measurement, MODIS satellite level 2

1. INTRODUCTION

Water vapor is considered as one of the most important greenhouse gases in the atmosphere of our planet. This parameter, that has a fast spatial and temporal variation, is a key factor in the study of the weather forecast and the climate system of the earth (Shi *et al.*, 2015). In addition, the delay caused by the tropospheric water vapor is one of the most influential errors that can disturb the GNSS signals and limit the performance of these systems. The troposphere delay introduces a positioning error on the transmitted satellite signals from about 2.5 m at the zenith to over 20 m at a lower elevation angle below 15°. This delay which has been considered for a long time as a critical problem for precise GNSS applications, is now used as a key parameter in the estimation of the IWV distribution, which is defined as the total atmospheric water vapor contained in an area of 1 m^2 (Shi *et al*,. 2015; Zheng *et al.*, 2018; Beldjilali & Benadda, 2016).

With the technological development of the GNSS systems in addition to many signals existing as open service for the GNSS users, various algorithms and methods have been developed to determine the *IWV* value using ground-based GNSS. Those algorithms used for monitoring the water vapor variation have experienced rapid development; actually, they can provide accurate estimates of *IWV* at high temporal resolution in any location and in all weather conditions. The studies presented in literature showed encouraging results concluded that the results obtained by the GNSS sensing have the same level of accuracy, with 2-mm root-mean-square (*RMS*) (Bevis *et al.,* 1992), as the traditional methods of sensing using Radiosonde measurements and microwave radiometers (Liu *et al.,* 2010; Li *et al.,* 2012b). Besides, the low cost and the portability of the GNSS base-ground make it an ideal method of atmospheric sensing especially in countries with limited technological resources.

Nowadays, with the rapid deployment of the GNSS monitoring station, a remarkable improvement in the GNSS network has been established by the IGS, and this network can be used in several weather prediction applications. The IGS real-time service (RTS) was officially launched on April 1st, 2013, and provides real-time products for GPS.

In this paper, we present an algorithm that uses the IGS data for the *IWV* estimation; precise IGS ephemeris and GPS correction models were used to calculate the *ZTD* values. The current accuracy level of precise GPS orbits from the IGS is sufficient to provide an estimation of *ZTD* with accuracy in the order of a few millimeters. In this work the zenith total delay calculated using a mapping function is the sum of Zenith Hydrostatic Delay and Zenith Wet Delay, the *ZHD* being estimated using one of the models developed as the Saastamoinen model (1972) or UNB3 model (University of New Brunswick tropospheric propagation delay model).

In the end, the relation between the *ZWD* and *IWV* is used to estimate the *IWV* value (Liu *et al.,* 2010; Yao & Zhao, 2016; Yuan *et al.,* 2014).

2. IGS DATA

The *ZTD* solutions are computed in different locations and times using our developed MATLAB program in the IGS data processing. The IGS stations used in this work are presented in Table 1.

Three types of RINEX files downloaded from IGS FTP service have been used in this work (Gurtner 2007):

- The first one is the navigation file (*. *n), which contains information about the satellite position (Orbital element), which helps to calculate the position and elevation of each satellite used by the mapping function to calculate the *ZTD*.
- The second one is an observation file (*. *o), which contains pseudo-distance between each satellite and the station (receiver antenna). The distance calculated by each code transmitted by each satellite is used by our algorithm to calculate the positions of each station. The position of a fixed station is a variable because of the errors that influence on the GPS signals.
- The third and last file is meteorological (*. *m); it contains the meteorological information (pressure, temperature, humidity) at the station level during the GPS measurement. It should be noted that not all IGS station contains meteorological information, for that we can use standard information, which provides accuracy similar to the one obtained from measured data. Also, we can use models to calculate these parameters in the sites based on near meteorological stations.

In the GPS positioning, two parameters are used to describe the quality of the results obtained: the precision and the accuracy. The precision is defined as the difference between the estimated and the true position. The accuracy can be explained as the closeness degree of the positions calculated to their mean in a static point. The GPS receivers' accuracies are generally estimated using the Root Mean Square (*RMS*) radial error statistic (Van Diggelen, 1998). According to the linear model of the position estimation and the characteristic of the errors, the *RMS* statistic error is related to the positional covariance matrix, the Root Mean Square Error (RMSE) is given by Sanz Subirana *et al.* (2013) :

$$RMS_{\Delta x} = \sqrt{trace\left(P_{\Delta x}\right)} \tag{1}$$

$$P_{\Delta x} = \sigma^2 \left(G^T G\right)^{-1} \tag{2}$$

$$RMS_{\Delta x} = \sigma \sqrt{trace\left[\left(G^T G\right)^{-1}\right]} \tag{3}$$

σ^2 is the variance and *G* is the geometry matrix. This equation for the *RMS* states that the trace of the matrix $(GT\ G)^{-1}$ is a scalar factor of the *RMS* σ and this matrix can be written as (Sanz Subirana *et al.*, 2013):

Table 1. Used station position

Station	City	Country	Lat	Lng	Alt
ANKR	Ankara	Turkey	39.88	32.75	974.8
CEBR	Cebreros	Spain	40.45	-4.36	775.8
GENO	Genova	Italy	44.41	08.92	137.0
ISTA	Istanbul	Turkey	41.10	29.01	147.2
MOSE	Roma	Italy	41.89	12.49	120.6
MEDI	Mediciana	Italy	44.51	11.64	050.0
MELI	Melilla	Spain	35.28	-2.95	093.0
NICO	Nicosia	Cyprus	35.14	33.39	155.0
NOT1	Noto	Italy	36.87	14.98	126.2
ORID	Ohrid	Macedonia	41.12	20.79	773.0
REDU	Redu	Belgium	50.00	05.14	369.9
WTZS	Koetzting	Germany	49.14	12.87	663.4

Table 2. Description of material installed on each station

	GNSS receiver		Meteor Sensors model		
Station	Receiver Type	Antenna	Humidity	Pressure	Temp
ANKR	LEICA GR30	LEIAR10	MP408A	APS 9215	MP408A-T4
CEBR	SEPT POLARX4	SEPCHOKE_MC	N	N	N
GENO	TRIMBLE 4700	TRM29659.00	N	N	N
ISTA	LEICA GR25	LEIAR25.R4	WXT520	WXT520	WXT520
M0SE	LEICA GR25	LEIAR25.R4	WXT520	WXT520	WXT520
MEDI	LEICA GR10	LEIAR20	N	N	N
MELI	LEICA GR10	LEIAR25.R4	N	N	N
NICO	LEICA GR25	LEIAR25.R4	MP408A	APS 9215	MP408A-T4
NOT1	LEICA GR30	LEIAR20	N	N	N
ORID	LEICA GRX1200	LEIAT504GG	MP408A	APS 9215	MP408A-T4
REDU	SEPTPOLARX4	SEPCHOKE_MC	N	N	N
WTZS	SEPTPOLARX4TR	LEIAR25.R3	MP 400A	DIGIQ	809 L 0-100

$$\left(G^T\ G\right)^{-1} = \sigma_{\Delta x} = \begin{bmatrix} \sigma_{xx} & \sigma_{xy} & \sigma_{xz} & \sigma_{xt} \\ \sigma_{xy} & \sigma_{yy} & \sigma_{yz} & \sigma_{yt} \\ \sigma_{xz} & \sigma_{yz} & \sigma_{zz} & \sigma_{zt} \\ \sigma_{xt} & \sigma_{yt} & \sigma_{zt} & \sigma_{tt} \end{bmatrix} \quad (4)$$

The variance (σ) of each position (x, y, z, t) can be predicted from the corresponding variances on the diagonal of the covariance matrix. The diagonal elements of matrix $P_{\Delta x}$ (σ_{xx}, σ_{yy}, σ_{zz}, σ_{tt}) represent the formal error of the estimated components vector (Sanz Subirana *et al.,* 2013):

$$\begin{cases} \sigma_{xx} = \sqrt{P_{xx}} \\ \sigma_{yy} = \sqrt{P_{yy}} \\ \sigma_{tt} = \sqrt{P_{zz}} \\ \sigma_{tt} = \sqrt{P_{tt}} \end{cases} \quad (5)$$

3. PROPOSED ALGORITHM

Figure 1 gives a detailed description of the proposed algorithm used to estimate the integrated water vapor from the IGS database.

Table 3. Used station *RMS* and Bias

	Winter		Spring		Summer		Autumn	
Station	RMS (cm)	Bias (m)	RMS (cm)	Bias (m)	RMS (cm)	Bias (m)	RMS (cm)	Bias (m)
ANKR	0.428	9.1364	0.351	8.6854	0.251	8.9696	0.323	9.5819
CEBR	0.231	1.0968	0.263	1.5692	0.295	1.6934	0.263	1.0712
GENO	0.499	2.0193	0.248	1.9651	0.286	2.0012	0.241	1.5852
ISTA	0.303	1.8687	0.200	1.6564	0.206	1.0617	0.290	1.6853
M0SE	3.254	2.356	5.985	3.4885	6.242	3.1205	5.086	3.4505
MEDI	0.234	1.8795	0.392	2.1933	0.148	2.1456	0.184	1.5412
MELI	0.213	1.1974	0.214	2.0839	0.270	2.1234	0.214	1.7183
NICO	0.268	3.2189	0.256	3.0133	0.211	2.2763	0.352	2.9412
NOT1	0.246	1.4751	0.249	1.7212	0.292	1.4348	0.190	1.7392
ORID	5.550	5.2535	5.436	5.1483	3.888	2.3493	4.460	2.9867
REDU	0.299	1.8722	0.292	2.1293	0.291	1.3636	0.190	1.3751
WTZS	0.300	1.7041	0.182	2.2368	0.181	1.1386	0.257	1.2603

The Rinex files are used to calculate the location of each station (latitude, longitude, and altitude), the elevation of each satellite is also calculated from this information. The satellite elevation is the key parameter to calculate the mapping function used to estimate the tropospheric zenith delay. The zenith dry delay is computed with the Saastamoinen (1972) model, which is based on the meteorological parameters, and the zenith wet delay is the result of subtracting the *ZHD* from the *ZTD*. Finally, the integrated water vapor value is estimated from the *ZWD* value using a transformation parameter (*Q*).

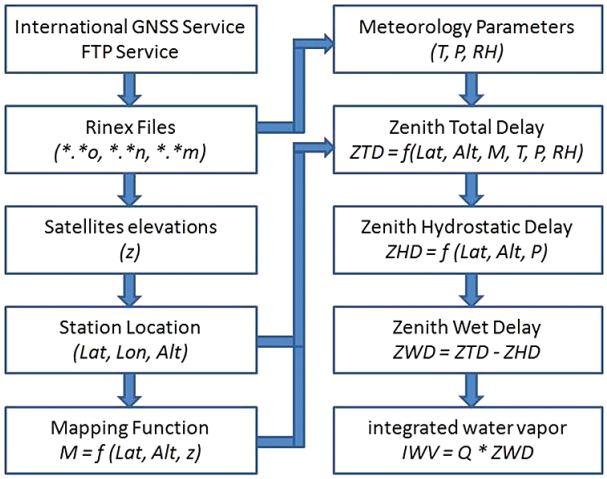

Fig. 1. Algorithm used to estimate *IWV*

4. METHODOLOGY AND RESULTS

The GNSS microwave signals transmitted from the satellites to the receivers propagate through different layers of the atmosphere are affected by many phenomena as the tropospheric effect. In this part of the atmosphere, the straight-line path will be converted to a curved path; this effect is due to the variation of the refraction index in the layer, related to the atmospheric variable (pressure, temperature, and relative humidity). The modification in the type of path causes a delay in the reception level named tropospheric zenith total delay, which can express as the integrated refractivity along a vertical path through the neutral atmosphere. This extra path length is given by Liu *et al.* (2010) and Klein Baltink *et al.* (2002):

$$ZTD = c\tau = 10^{-6}\int_{0}^{\infty} N(h)\,dh \qquad (6)$$

where *c* is the speed of light in vacuum τ is the delay measured in units of time and *N*(*h*) is the refractive index as a function of position (*h*) along the curved ray path. This refractivity of the atmosphere is a function of its temperature, pressure and water vapor pressure, it can be written also as (Boccolari *et al.,* 2002; Essen, 1953; Thayer, 1974):

$$N = k_1\left(\frac{P_d}{T}\right)Z_d^{-1} + k_2\left(\frac{P_v}{T}\right)Z_v^{-1} + k_3\left(\frac{P_v}{T^2}\right)Z_v^{-1} \qquad (7)$$

P_d is the partial pressure of dry air (in hPa), P_v is the partial pressure of water vapor (in hPa), *T* is the total atmospheric temperature (in degrees Kelvin) Z_d^{-1} is the inverse compressibility factors for dry air and Z_v^{-1} is the inverse compressibility factors for water vapor (Klein Baltink *et al.,* 2002; Essen, 1953) . The constants k_1, k_2 and k_3 are presented by Thayer (1974):

$k_1 = (77.64 \pm 0.014)$ $\quad KhPa^{-1}$

$k_2 = (64.79 \pm 0.080)$ $\quad hPa^{-1}$

$k_3 = (3.776 \pm 0.004)10^5\ K^2hPa^{-1}$

The uncertainties in the constant values used in this equation reduce the precision of the final result obtained; the refractivity has an error of 2% (Liu *et al.,* 2010). The function of the refractive index can be also expressed by the following simplified equation:

$$N = k_1\rho + k_2\frac{P_v}{Z_v T} + k_3\frac{P_v}{Z_v T^2} \qquad (8)$$

ρ is the total mass density of the atmosphere.

There are several approximated versions of the equation for the estimation of the refractive index; among these equations we selected the following one (Kirchengast *et al.,* 2004) :

$$N = 77.6\frac{P}{T} + 3.73\ 10^5\frac{P_v}{T^2} \qquad (9)$$

P is the total atmospheric pressure.

This expression has an accuracy of 5% under normal atmospheric conditions (Kirchengast *et al.,* 2004) .

Saastamoinen (1972) explained that the *ZTD* is composed by two different components, a hydrostatic or dry delay which represents the dominant part of the *ZTD* (caused by the effects of dry gas) and wet delay caused by the atmospheric water vapor which represent a small quantity (Takeiki *et al.,* 2010) :

$$ZTD = ZWD + ZHD \qquad (10)$$

The Zenith Total Delay along the zenith direction for a path depends on the elevation angle. The *ZTD* can be computed from the hydrostatic and the wet zenith delays by:

$$ZTD = ZHD \cdot m_h(z) + ZWD \cdot m_w(z) \qquad (11)$$

where $m_h(z)$ is hydrostatic mapping is function and $m_w(z)$ is the wet mapping function. Many models have been developed to estimate these functions (Takeiki *et al.,* 2010; Norazmi *et al.,* 2015). The difference between these models is the number of the input parameters, especially the meteorological parameters; some functions use three parameters, including the surface temperature, pressure and relative humidity. Also, there are others functions that are based on pressure only. The last types of mapping functions are approximated functions that use climatological value of atmospheric parameters. In this work we used satellites with an elevation above 15°, because many studies in literature concluded that lower elevation angles may cause significant errors (Liu *et al.,*2010; Jin *et al.,* 2014).

In this work we used the Herring Mapping Function, developed in 1992, which is based on the Marini's coefficients *a*, *b*, and *c* (Marini, 1972). These coefficients are calculated based on the location parameters (latitude and elevation), in addition to the surface temperature. The mapping function is inversely proportional to the elevation angle (*z*), as shown in equation (12) (Jin *et al.,* 2014; Herring, 1992).

$$m(z)=\frac{1+\dfrac{a}{1+\dfrac{b}{1+c}}}{\sin z+\dfrac{a}{\sin z+\dfrac{b}{\sin z+c}}} \quad (12)$$

The coefficients *a*, *b* and *c* are calculated using the following equations (Marini, 1972) :

$a = [1.2320 + 0.0130 \cos\varphi - 0.0209H + 0.00215(T_s - 10)]10^{-3}$
$b = [3.1612 - 0.1600 \cos\varphi - 0.0331H + 0.00206(T_s - 10)]10^{-3}$
$c = [71.244 - 4.2930 \cos\varphi - 0.1490H + 0.00210(T_s - 10)]10^{-34}$

φ is the site latitude in degrees. *H* is the station elevation in Km. T_s is the surface temperature.

The following table shows the 12 stations *ZTD* variation in the different seasons. The results were processed in MATLAB program using the Saastamoinen model and the Herring Mapping Function based on the satellites elevation (Table 4).

The value of the integrated water vapor is related to the wet delay. To estimate it, firstly the value of hydrostatic delay should be known, as the GPS data can deliver only the tropospheric zenith total delay. The next step is to calculate the *ZHD* value and the *ZWD* can then be computed by subtracting the *ZHD* from the observed *ZTD*. The zenith dry delay model in millimeters, due to the effects of dry gases can be calculated from surface pressure P_s only (Namaoui *et al.,* 2017):

$$ZHD = 10^{-6}\frac{k_1 R_d P_s}{g_m} \quad (13)$$

R_d is the gas constant of dry air. g_m is the mean gravity. Using experimental observations, the *ZHD* developed by Saastamoinen in 1972 is given by Shi *et al,.* (2015) and Tregoning & Herring (2006):

$$ZHD = \frac{2.2779 P_s}{1-0.00266\cos 2\varphi - 0.00028H} \quad (14)$$

With the precise pressure data *Ps* at the user location, the *ZHD* can be precisely calculated with up to 0.2 mm accuracy (Bevis *et al.,* 1992). The next step is to estimate the *ZWD*:

$$ZWD = ZTD - ZHD \quad (15)$$

Based on the Saastamoinen model (1972) and the parameters as described in figure 1, the zenith wet delay is calculated for each station. To estimate water vapor information from *ZWD*, the conversion constant must be calculated. This constant will be multiplied by the *ZWD* as (Shi *et al.,* 2015):

$$IWV = Q\,ZVD \quad (16)$$

IWV is defined as the water vapor quantity in unit of Kg/m² and *Q* is the transfer value and it is written as (Beldjilali & Benadda, 2016):

$$Q \approx \frac{3.75410^{-3}\int_0^{\infty}\dfrac{e(h)}{T(h)^2}dh}{\int_0^{\infty}\rho_v(h)dh} = 10^6\left[R_v\left(\frac{k_3}{T_M}+k_2'\right)\right]^{-1} \quad (17)$$

R_v is the gas constant for water vapor: R_v = 461.51 $JKg^{-1}K^{-1}$; ρ_v is the absolute humidity in kg/m^3

The constant k'_2 is calculated using the following equation:

$$k_2' = k_2 - \frac{M_w}{M_d} \quad (18)$$

where M_w is the molar mass of water vapor and M_d is the molar mass of dry air, the constant k'_2 is equal to 22 $KhPa^{-1}$.

Table 4. Seasonal *ZTD* variation (in meters) at 12 IGS station

	Winter			Spring			Summer			Autumn		
Station	min	max	mean	Min	max	mean	min	max	mean	min	max	mean
ANKR	1.94	2.21	2.11	2.03	2.21	2.07	2.08	2.19	2.16	2.01	2.23	2.04
CEBR	2.06	2.31	2.15	2.08	2.27	2.20	2.06	2.25	2.15	2.05	2.30	2.18
GENO	2.10	2.42	2.32	2.29	2.63	2.47	2.28	2.54	2.41	2.21	2.56	2.42
ISTA	2.16	2.43	2.32	2.21	2.48	2.37	2.23	2.50	2.45	2.22	2.48	2.40
MOSE	2.06	2.25	2.15	2.25	2.54	2.31	2.28	2.45	2.38	2.19	2.41	2.25
MEDI	2.03	2.40	2.23	2.23	2.70	2.49	2.33	2.47	2.40	2.22	2.43	2.28
MELI	2.24	2.50	2.38	2.29	2.62	2.43	2.26	2.53	2.40	2.30	2.75	2.50
NICO	2.15	2.51	2.37	2.37	2.57	2.48	2.29	2.42	2.32	2.28	2.57	2.44
NOT1	2.19	2.60	2.38	2.19	2.60	2.40	2.25	2.49	2.33	2.21	2.48	2.35
ORID	1.91	2.19	2.09	2.02	2.26	2.12	2.03	2.26	2.17	2.05	2.23	2.16
REDU	1.97	2.28	2.14	2.20	2.34	2.29	2.23	2.34	2.28	2.17	2.31	2.23
WTZS	1.90	2.23	2.06	2.08	2.27	2.16	2.17	2.27	2.23	2.25	2.04	2.17

T_M is the weighted mean temperature of the atmosphere in Kelvin defined as (Davis *et al.,* 1985):

$$T_M = \frac{\int\left(\frac{e(h)}{T(h)}\right)dh}{\int\left(\frac{e(h)}{T(h)^2}\right)dh} \quad (19)$$

where $e(h)$ is the vapor pressure, T is the absolute temperature, and dh is the integral path. The relationship between surface temperature T_s and T_M can be introduced through the linear regression function (Bevis *et al.*. 1992):

$$T_M = 0.72\,T_s + 70.2 \quad (20)$$

According to Table 5 it can be clearly seen that the stations in the coastal areas has a value of water vapor concentration much larger than the stations farther away from the Mediterranean (WTZS, REDU, ORID and ANKR). For example, the average winter IWV values in inland area is between 12 and 16 Kg/m^2 while its values for stations in the coastal area are above 20 Kg/m^2 and can reach 30 Kg/m^2.

It should be also noted that generally for all stations, the winter season has the minimum values of the IWV compared to others times of the year. On the other hand, the seasons of spring and summer show the maximum levels of the water vapor.

5. RESULTS VALIDATION BY RADIOSONDE

Radiosondes are equipped with instruments capable of measuring profiles of atmospheric temperature, pressure, and relative humidity, additionally to the wind parameters (speed and direction) at different altitudes along the flight path (Berezin *et al.,* 2016). Using these parameters, Radiosondes provide a good way to measure the residual tropospheric delay and estimate the integrated water vapor in the atmosphere. However, these devices are relatively expensive and offer limited measurements, usually Radiosonde are launched twice a day with a 12-h interval at 00:00 and 12:00 UTC (Ha *et al.,* 2010; Vásquez Becerra & Grejner-Brzezinska, 2013) .

The integrated water vapor amount is obtained as (Singh *et al.,* 2014; Chrysoulakis & Cartalis, 2002) :

$$IWV = \frac{1}{g_m}\int_{p_s}^{0} M_r d_p = \frac{1}{g_m}\sum_{i=1}^{n}\left(\frac{M_{r_i} + M_{r_{i+1}}}{2}\right)\left(p_i - p_{i+1}\right) \quad (21)$$

where M_r is the mixing ratio, p_i the pressure at ith level of altitude.

According to literature it is possible also, to calculate the total amount of water vapor between two altitudes by integrating the measurements of the water vapor density between these two altitudes as (Realini *et al.,* 2014):

$$IWV = \int_{h_1}^{h_2} r_{wv}(h)\,dh \quad (22)$$

where h_1 is the ground altitude and h_2 is the max altitude of the atmospheric layer and ρ_{wv} is the water vapor mass density at altitude h.

The value of h_2 is chosen in such a way as to measure the maximum quantity of water vapor contained in a shortest path.. It is proved that 95% of the total accumulated water vapor is found at altitudes below 10 km, above this altitude the water vapor content can be neglected (Schüler *et al.,* 2000; Hopfield, 1971).

ρ_{wv} is a function of the relative humidity and temperature, and it can be written as:

$$\rho_{wv} = RHe\frac{1}{R_v T} \quad (23)$$

The integrated water vapor is proportional to the humidity value, the error in the IWV measurement depends on the

Table 5. *IWV* variation (in Kg/m^2) of the 12 stations in different seasons

	Winter			Spring			Summer			Autumn		
Station	min	max	mean	Min	max	mean	min	max	mean	min	max	mean
ANKR	5.8	19.8	14.8	10.4	22.3	18.5	13.3	18.8	17.3	09.6	20.9	11.3
CEBR	12.2	24.6	16.4	13.2	26.4	19.0	12.3	21.6	16.4	11.7	24.1	18.3
GENO	13.9	30.1	25.1	23.2	40.4	32.7	23.1	36.5	29.6	19.4	37.2	30.1
ISTA	16.9	30.4	25.0	16.4	33.2	27.6	20.7	34.2	31.7	20.1	33.3	29.3
MOSE	11.2	24.8	18.5	21.7	36.4	25.2	23.2	31.9	28.3	19.0	30.1	21.9
MEDI	10.2	28.9	20.2	20.6	44.4	33.9	25.5	32.5	29.5	20.3	30.9	23.1
MELI	21.1	34.2	28.1	23.5	40.6	31.0	22.5	35.9	29.2	24.2	46.7	34.2
NICO	16.5	34.4	27.3	27.5	38.1	33.5	23.7	30.5	25.4	23.4	37.9	31.2
NOT1	18.4	39.4	28.4	18.7	39.5	29.6	21.8	34.1	26.1	19.7	33.6	26.7
ORID	4.1	18.1	13.1	09.6	21.9	15.2	10.03	22.0	17.7	11.6	20.8	16.9
REDU	7.1	22.8	15.6	19.2	26.2	23.7	20.8	25.9	23.0	17.4	24.5	20.5
WTZS	3.9	20.7	12.3	13.3	23.2	17.7	17.8	23.1	20.9	11.5	21.9	17.9

precision of the humidity (*RH*) estimation along the path, generally the mean Radiosonde measurement error vary between 5% and 10 % of the real value (Berezin *et al.,* 2016).

The data of the Radiosonde used in this work have been downloaded from the University of Wyoming website (http://weather.uwyo.edu/upperair/sounding.html). In this paper they provide real values of the IWV, and are taken as reference value to validate the result of the IWV values calculated by our algorithm using GPS data.

Figure 2 gives information about the Radiosonde station used in this work to validate the IWV value obtained by the GPS signal measurement. This station located in Rome is near to the M0SE IGS station.

6. MODIS SATELLITE IMAGE

To remotely sense the earth Atmosphere, Ocean and Land, two Moderate Resolution Imaging Spectro-radiometer (MODIS) instruments are implemented on the NASA's (National Aeronautics and Space Administration) Earth Observation System. The Terra EOS AM-1 platform launched on December 18, 1999 and the Aqua EOS PM-1 platform launched on May 4, 2002. They provide passively high radiometric sensitivity observation of electromagnetic radiation in 36 visible IR spectral bands between 0.4µm and 14.4µm. The two instruments are in polar sun-synchronous orbit at an altitude of 705 km, and the swath width of the MODIS data for them is 2300 and 2330 km, respectively with a resolution in the IR of 1 x 1 km. To remotely sense the atmospheric water vapor both Terra and Aqua MODIS have one channel centered at 0.94µm. The advantage of using this wave length came from its strong water vapor absorption occurs (Gao *et al.*, 2003 ; Gao & Li, 2008; Chang & Jin, 2013; Chang *et al.*, 2014; Reis *et al.,* 2015).

Table 6. The near IR cannel used in the water vapor remote sensing

MODIS Cannel	Wave length (µm)
2	0.865
5	1.24
17	0.905
18	0.936
19	0.940

Water vapor can be derived using differentiating channels on and off absorption bands. In the case of MODIS satellite, to derive the atmospheric transmittances, two radiance channels with 865 and 940 nm wavelength are used (Gao & Li, 2008).

$$\frac{\rho_{940}}{\rho_{865}} = e^{\alpha+\beta(W^*)/2} \tag{24}$$

ρ_{940} and ρ_{865} are the atmospheric transmittances near 940 and 865nm. α, β are constant; W^* is the derived total water vapor amount. The vertical column water vapor amount converted from W^*, based on the solar and the observational geometries can be calculated using the following equation (Liu *et al.,* 2006):

$$IWV = \frac{W^*}{\frac{1}{cos(\theta s)} + \frac{1}{cos(\theta v)}} \tag{25}$$

θ_s is the solar zenith angle, and θ_v is the view zenith angle.

The atmospheric transmittances can be calculated based on the Radiation measured at the sensor

$$L_{sen}(\lambda) = L_{sun}(\lambda)T(\lambda)\rho(\lambda) + L_{path}(\lambda) \tag{26}$$

λ is the wavelength, L_{sen} is the radiation measured by the sensor, L_{sun} is the solar radiation above the atmosphere, T is the total atmospheric transmittance and L_{path} is the path scattered radiance.

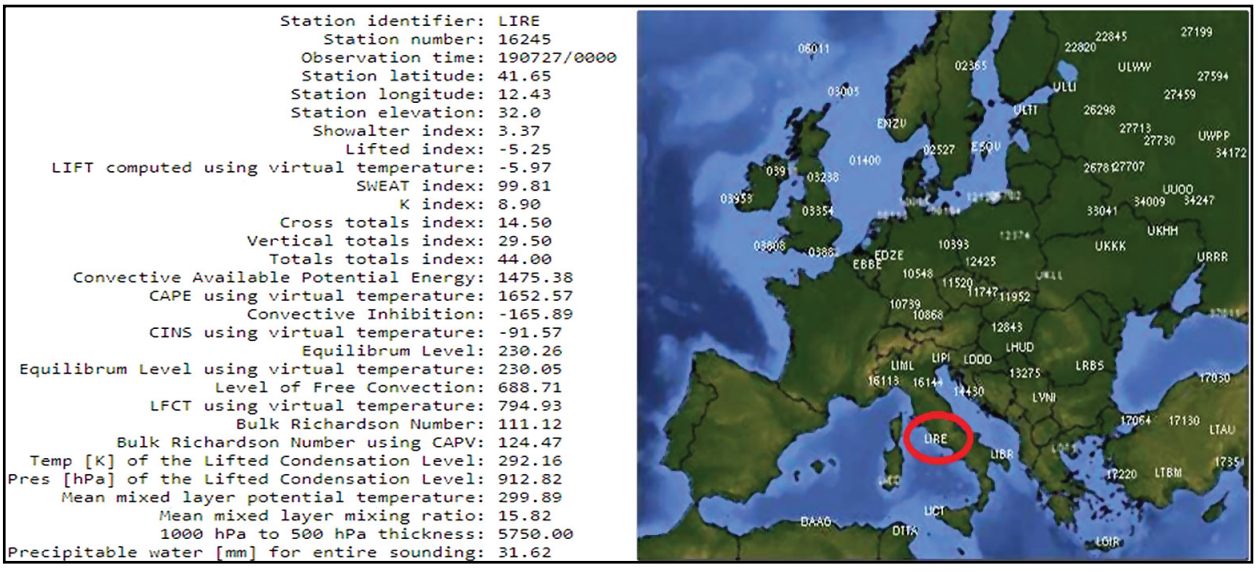

```
                    Station identifier: LIRE
                        Station number: 16245
                      Observation time: 190727/0000
                      Station latitude: 41.65
                     Station longitude: 12.43
                     Station elevation: 32.0
                       Showalter index: 3.37
                          Lifted index: -5.25
LIFT computed using virtual temperature: -5.97
                          SWEAT index: 99.81
                              K index: 8.90
                    Cross totals index: 14.50
                  Vertical totals index: 29.50
                    Totals totals index: 44.00
  Convective Available Potential Energy: 1475.38
        CAPE using virtual temperature: 1652.57
                  Convective Inhibition: -165.89
        CINS using virtual temperature: -91.57
                      Equilibrum Level: 230.26
Equilibrum Level using virtual temperature: 230.05
             Level of Free Convection: 688.71
        LFCT using virtual temperature: 794.93
                 Bulk Richardson Number: 111.12
      Bulk Richardson Number using CAPV: 124.47
Temp [K] of the Lifted Condensation Level: 292.16
Pres [hPa] of the Lifted Condensation Level: 912.82
 Mean mixed layer potential temperature: 299.89
          Mean mixed layer mixing ratio: 15.82
          1000 hPa to 500 hPa thickness: 5750.00
Precipitable water [mm] for entire sounding: 31.62
```

Fig. 2. Station information (LIRE 16245)

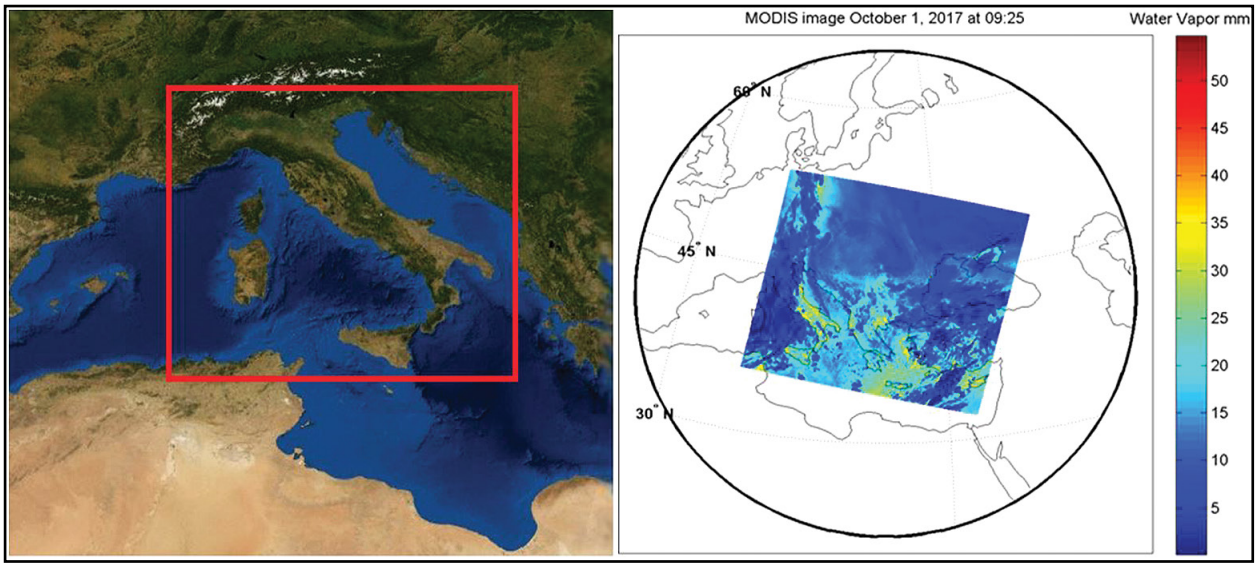

Fig. 3. The study region with the MODIS (resolution of 1×1 Km)

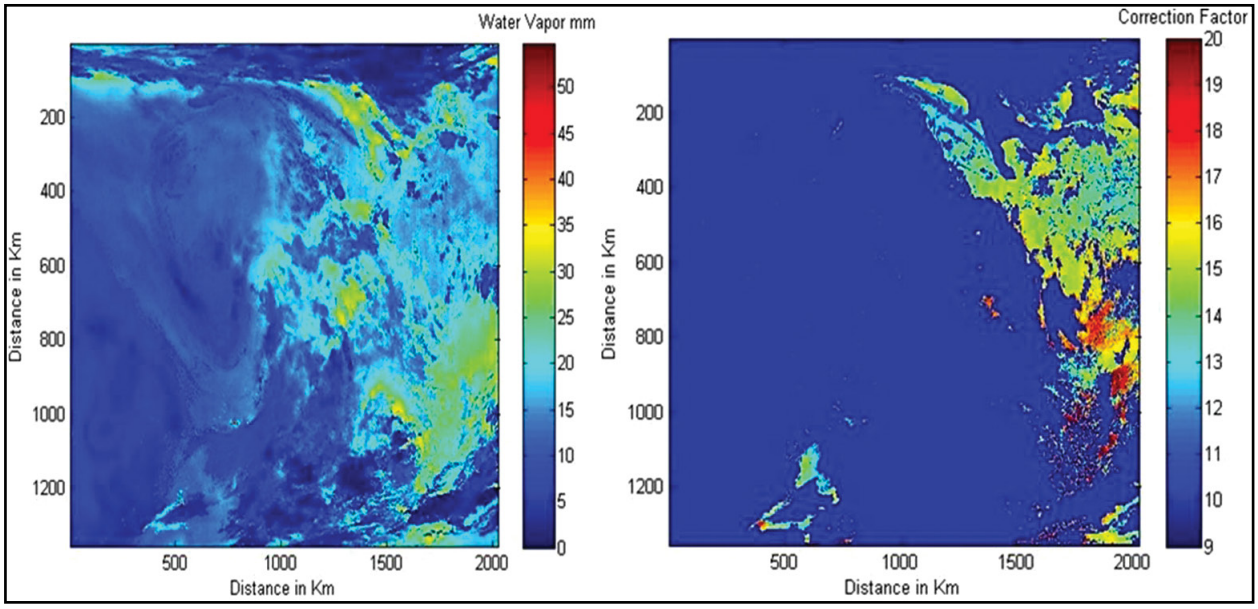

Fig. 4. Water Vapor distribution and the correction factor

For this paper we used our own MATLAB code to process the MODIS data. Two files are used in this work, the MOD05_L2 file that contains water vapor estimated by near-IR and IR sensing and the MOD03 file that contains geographical information.

7. COMPARISON

The radiosonde measurement and MODIS satellite are able to estimate the amount of atmospheric water vapor with high precision. These two instruments can be considered as ideal tools to analyze the accuracy of the temporal and spatial variation of the water vapor values delivered by the GPS stations. Figure 5 shows a comparison between the IWV values computed by our algorithm (GPS) and the values delivered from the Radiosonde (left panel) and the values delivered from MODIS satellite (right panel)

According to figures 5 and 6, we can conclude that, for this station (M0SE Rome), the difference between the two solutions (GPS and Radiosonde) in the 94% of case is less than 3 mm; in some case the *RMS* can achieve 4 mm. The two solutions have a monthly *RMS* of 1.54 and a correlation of 95.37%. For the selected station (M0SE, Rome) the spatial variation of the water vapor is shown in figure 7.

To compare the MODIS water vapor values with the ones delivered by GPS we focus on the Rome IGS station (41.89, 12.49). The results show high correlation (73%) with differences smaller than 4 mm in 65% of time.

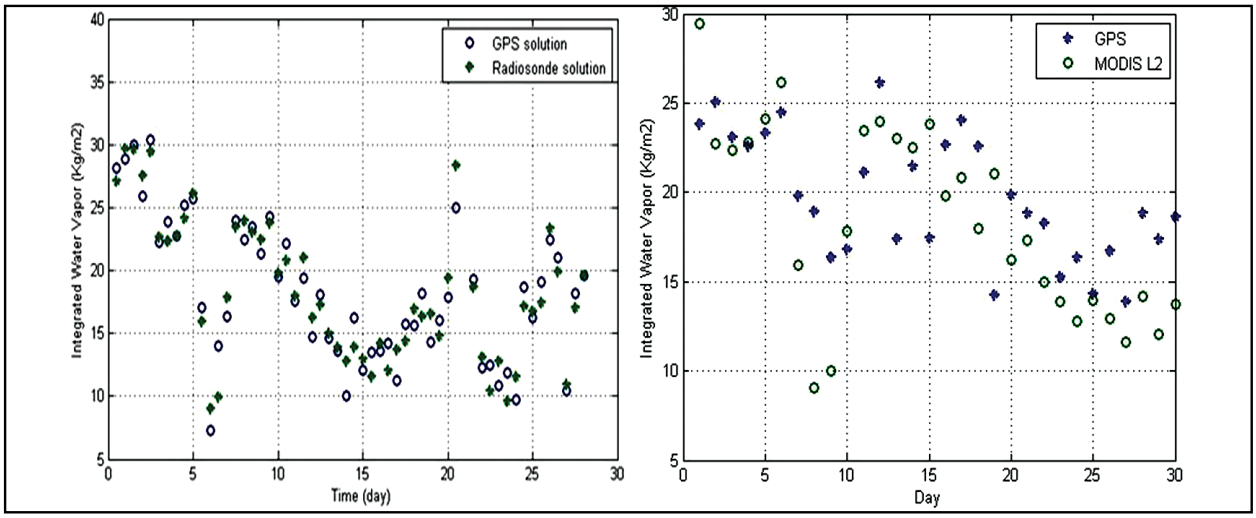

Fig. 5. Daily *IWV* from GPS, Radiosonde and MODIS solution (October, M0SE, Rome)

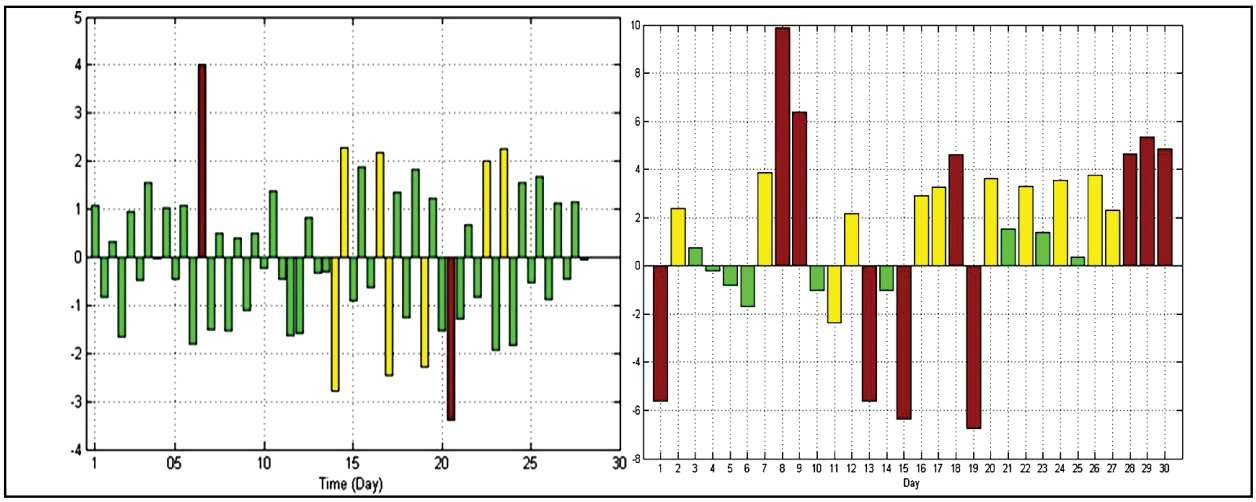

Fig. 6. Daily *RMS* variation between solutions (October, M0SE, Rome)

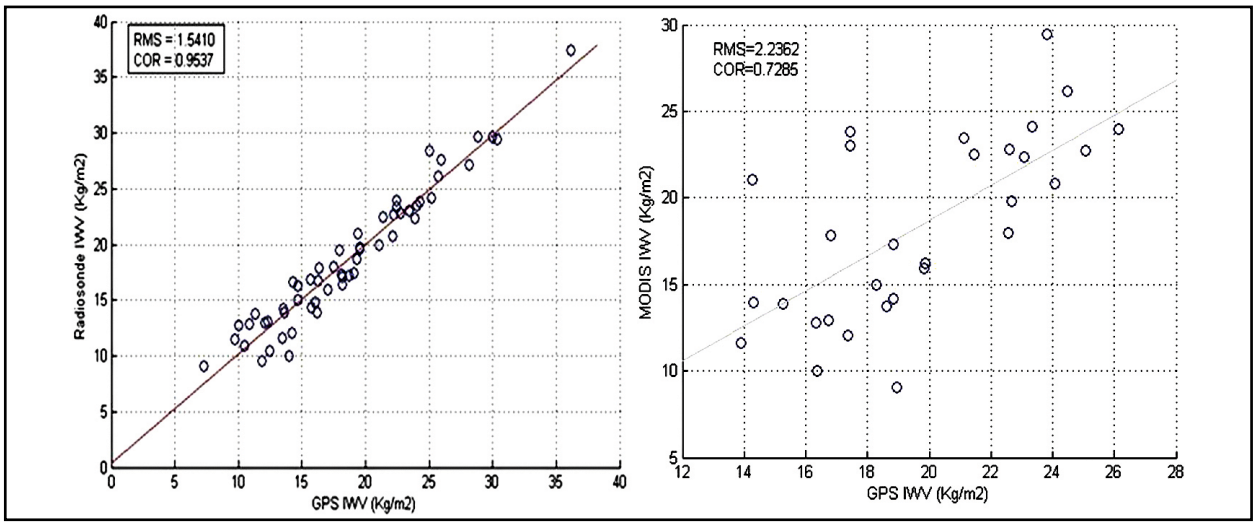

Fig. 7. Scatter plot between solutions (October, M0SE, Rome)

The degradation in the correlation rate between MODIS and GPS is caused by the spatial resolution. The data from MODIS have resolution of 1x1Km while GPS resolution is 20x20 km.

8. CONCLUSION

In this paper, a study on the IWV space and time variation was presented. Data from 12 IGS stations were used; the aim of using these stations is to assure the largest coverage of the Mediterranean area in the four seasons of the year. The relation between the integrated water vapor and the delay introduced on the GPS signals propagation were investigated. The relations between the IWV and the GPS signal delay established by the Saastamoinen model were compared to derived estimates obtained from Radiosondes and MODIS data. The results presented show that the IWV values obtained by the GPS solution is highly correlated with those obtained from Radiosonde measurements and MODIS data. The advantage of using GPS data is the higher temporal resolutions and spatial coverage compared to the other data sources, which allows for observations only twice a day, and in the case of Radiosondes, have limited spatial coverage.

REFERENCES

Beldjilali B., Benadda B. (2016). Optimized station to estimate atmospheric integrated water vapor levels using GNSS signals and meteorology parameters. *ETRI Journal*, **38**(*6*): 1172-1178, https://doi.org/10.4218/etrij.16.0116.0093

Berezin I.A., Timofeyev Yu.M., Virolainen Ya.A., Volkova K.A. (2016). Comparison of ground-based microwave measurements of precipitable water vapor with radiosounding data. *Atmospheric and Oceanic Optics*, **29**(*3*): 274–281, https://doi.org/10.1134/S1024856016030040

Bevis M., Businger S., Herring T.A., Rocken C., Anthes A., Ware R. H. (1992). GPS meteorology: Remote sensing of atmospheric water vapor using the global positioning system. *Journal of Geophysical research*, *Atmospheres*, **97**(*D14*): 15787-15801. https://doi.org/10.1029/92JD01517

Boccolari M., Fazlagic S., Frontero P., Lombroso L., Pugnaghi S., Santangelo R., Corradini S., Teggi S. (2002). GPS zenith total delays and precipitable water in comparison with special meteorological observations in Verona (Italy) during MAP-SOP. *Annals of geophysics*, **45**(*5*), https://doi.org/10.4401/ag-3534

Chang L., Jin S. (2013). MODIS infrared (IR) water vapor calibration model and assessment. *21st International Conference on Geoinformatics (GEOINFORMATICS*), Kaifeng, 2013, https://doi.org/10.1109/Geoinformatics.2013.6626197

Chang L., Jin S., He X. (2014). Assessment of InSAR atmospheric correction using both MODIS near-infrared and infrared water vapor products. *IEEE Transactions on Geoscience and Remote Sensing*, **52**(*9*): 5726-5735, https://doi.org/10.1109/TGRS.2013.2292070

Chrysoulakis N., Cartalis C. (2002). Improving the estimation of land surface temperature for the region of Greece: Adjustment of a split window algorithm to account for the distribution of precipitable water. *International Journal of Remote Sensing*, **23**(*5*): 871-880, Published online: 25 Nov 2010, https://doi.org/10.1080/01431160110071905

Davis J.L. Herring T.A., Shapiro I.I., Rogers A.E.E., Elgered G. (1985). Geodesy by radio interferometry: Effects of atmospheric modeling errors on estimates of baseline length. *Radio Science*, **20**(*6*): 1593-1607. https://doi.org/10.1029/RS020i006p01593

Essen L. (1953). The refractive indices of water vapour, air, oxygen, nitrogen, hydrogen, deuterium and helium. *Proceedings of the Physical Society*, **B66**(*3*): 189-193.

Gao B.-C., Li R. (2008). The time series of Terra and Aqua MODIS near-IR water vapor products. *IEEE International Geoscience and Remote Sensing Symposium (IGARSS)*, Boston, MA, 2008, III186-III189, https://doi.org/10.1109/IGARSS.2008.4779314

Gao B.-C., Yang P., Guo G., Park S.K,, Wiscombe W.J., Chen B. (2003). Measurements of water vapor and high clouds over the Tibetan Plateau with the Terra MODIS instrument, *IEEE Transactions on Geoscience and Remote Sensing*, **41**(*4*): 895-900, https://doi.org/10.1109/TGRS.2003.810704

Gurtner W. (2007). RINEX: The Receiver Independent Exchange Format, Version 3.00, Astronomical Institute, University of Bern.

Ha J., Park KD., Kim K. (2010). Comparison of atmospheric water vapor profiles obtained by GPS, MWR and radiosonde. *Asia-Pacific Journal of Atmospheric Science,* **46**(*3*): 233–241, https://doi.org/10.1007/s13143-010-1012-1

Herring T.A. (1992). Modelling atmospheric delays in the analysis of space geodetic data. *Proc. Symp. on Refraction of Transatmospheric Signals in Geodesy*, The Hague, The Netherlands, May 19-22, Netherlands Geodetic Commission, Publ, on Geodesy, New series, **36**: 157-164.

Hopfield H.S. (1971). Tropospheric effect on electromagnetically measured range: prediction from surface weather data. *Radio Science*, **6**(*3*): 357–367. https://doi.org/10.1029/RS006i003p00357

Jin S.G., Cardellach E., Xie F. (2014). GNSS Remote Sensing. Theory, Methods and Applications. Springer, Netherlands, 276 p.

Kirchengast G., Foelsche U., Steiner A. (2004). Occultations for Probing Atmosphere and Climate. Springer-Verlag Berlin Heidelberg, 408 p., https://doi.org/10.1007/978-3-662-09041-1

Klein Baltink H., van der Marel H., van der Hoeven A.G.A. (2002). Integrated atmospheric water vapor estimates from a regional GPS network. *Journal of Geophysical Research*, *Atmospheres*, **107**(*D3*): 3-8, https://doi.org/10.1029/2000JD000094

Li C., Liu Y., Zhu R. (2012a). An improved algorithm for retrieving atmospheric water vapor using MODIS near-infrared data. *2nd International Conference on Remote Sensing, Environment and Transportation Engineering*, Nanjing, 2012, 1-4, https://doi.org/10.1109/RSETE.2012.6260383

Li W., Yuan Y., Ou J., Li H., Li Z. (2012b). A new global zenith tropospheric delay model IGGtrop for GNSS applications. *Chinese Science Bulletin* **57**(*17*): 2132–2139, https://doi.org/10.1007/s11434-012-5010-9

Liu S., Zhang C., Guo X., Chu Y., Ge D., Fan J. (2006). Comparison of MODIS Atmospheric Water Vapor Retrieval, Meteorological Models Tropospheric Delay Estimation with the Results Derived from GPS. *IEEE International Symposium on Geoscience and Remote Sensing*, Denver, CO, 2006: 2615-2618, https://doi.org/10.1109/IGARSS.2006.675

Liu X., Yang Q, Cheng B., Xia B., Wang Y. (2010). Application of remote sensing water vapor based on GPS in the heavy rainfall. *The 2nd Conference on Environmental Science and Information Application Technology (ESIAT)*, Wuhan, 2010: 344-347, https://doi.org/10.1109/ESIAT.2010.5568575

Marini J.W. (1972). Correction of satellite tracking data for an arbitrary tropospheric profile. *Radio Science*, **7**(*2*): 223-231. https://doi.org/10.1029/RS007i002p00223

Namaoui H., Kahlouche S., Belbachir A.H., Van Malderen R., Brenot H., Pottiaux E. (2017). GPS water vapor and its comparison with radiosonde and ERA-Interim data in Algeria. *Adv. Atmos. Sci.*, **34**: 623–634, https://doi.org/10.1007/s00376-016-6111-1

Norazmi, M.F.B., Opaluwa, Y.D., Musa, T.A., Othman R. (2015). The Concept of Operational Near Real-Time GNSS Meteorology System for Atmospheric Water Vapour Monitoring over Peninsular Malaysia. *Arabian Journal for Science and Engineering*, **40**(*1*): 235–244, https://doi.org/10.1007/s13369-014-1481-0

Realini E., Sato K., Tsuda T., Susilo S., Manik T. (2014). An observation campaign of precipitable water vapor with multiple GPS receivers in western Java, Indonesia. *Prog. in Earth and Planet. Sci.* **1**(*17*). https://doi.org/10.1186/2197-4284-1-17

Reis A.R., Catalão J., Vieira G., Nico G. (2015). Mitigation of atmospheric phase delay in InSAR time series using ERA-interim model, GPS and MODIS data: Application to the permafrost deformation in Hurd Peninsula, Antarctica. *IEEE International Geoscience and Remote Sensing Symposium (IGARSS)*, Milan, 2015: 3454-3457, https://doi.org/10.1109/IGARSS.2015.7326563

Sanz Subirana J., Zornoza J.M.J., Hernández-Pajares M. (2013). GNSS data processing: Vol. I: Fundamentals and Algorithms. ESA TM-23/1, *ESA Communications*, ISBN: 978-92-9221-886-7, 238 p.

Schüler T., Hein G.W., Fissfeller B. (2000). Improved tropospheric delay modeling using an integrated approach of numerical weather models and GPS. *13th Int. Tech. Meeting of the Satellite Division of the U.S.Inst. of Navigation, ION GPS*, Salt Lake City, UT, 19-22 September, 600-615.

Shi J., Xu C., Guo J., Gao Y. (2015). Real-time GPS precise point positioning-based precipitable water vapor estimation for rainfall monitoring and forecasting. *IEEE Transactions on Geoscience and Remote Sensing Society*, **53** (*6*): 3452-3459, https://doi.org/10.1109/TGRS.2014.2377041

Singh D., Ghosh J.K., Kashyap D. (2014). Precipitable water vapor estimation in India from GPS-derived zenith delays using radiosonde data. *Meteorology and Atmospheric Physics,* **123**: 209–220, https://doi.org/10.1007/s00703-013-0293-1

Takeichi, N., Sakai, T., Fukushima, S., Ito K. (2010). Tropospheric delay correction with dense GPS network in L1-SAIF augmentation. *GPS Solutions,* **14**(*2*): 185–192, https://doi.org/10.1007/s10291-009-0133-4

Thayer G.D. (1974). An improved equation for the radio refractive index of air. *Radio Science*, **9**(*10*): 803-807. https://doi.org/10.1029/RS009i010p00803

Tregoning P., Herring T.A. (2006). Impact of a priori zenith hydrostatic delay errors on GPS estimates of station heights and zenith total delays. *Geophysical Research Letters*, **33**(*23*): 1-5, https://doi.org/10.1029/2006GL027706

Van Diggelen F. (1998). GPS accuracy: lies, damn lies, and statistics, *GPS World*, Nov. 29, 1998 (five pages).

Vázquez Becerra G.E., Grejner-Brzezinska, D.A. (2013). GPS-PWV estimation and validation with radiosonde data and numerical weather prediction model in Antarctica. *GPS Solution*, **17**: 29-39, https://doi.org/10.1007/s10291-012-0258-8

Yao Y., Zhao Q. (2016). Maximally using GPS observation for water vapor tomography, *IEEE Transactions on Geoscience and Remote Sensing*, **54**(*12*): 7185-7196, https://doi.org/10.1109/TGRS.2016.2597241

Yuan Y., Zhang K., Rohm W., Choy S., Norman R., Wang C,-S. (2014). Real-time retrieval of precipitable water vapor from GPS precise point positioning. *Journal of Geophysical Research, Atmospheres*, **119**(*16*): 10044-10057. https://doi.org/10.1002/2014jd021

Zheng, F., Lou, Y., Gu, S., Gong X., Shi C, (2018). Modeling tropospheric wet delays with national GNSS reference network in China for BeiDou precise point positioning. *Journal of Geodesy,* **92**(*5*): 545–560. https://doi.org/10.1007/s00190-017-1080-4